Homology modeling identifies crucial amino-acid residues that confer higher Na+ transport capacity of OcHKT1;5 from Oryza coarctata Roxb

Suji Somasundaram, Anne-Aliénor Véry, Rithvik S Vinekar, Tetsuya Ishikawa, Kumkum Kumari, Shalini Pulipati, Kavitha Kumaresan, Claire Corratgé-Faillie, R Sowdhamini, Ajay Parida, et al.

Homology modeling identifies crucial amino-acid residues that confer higher Na^+ transport capacity of OcHKT1;5 from *Oryza coarctata* Roxb.

Running Title: OcHKT1;5 has higher Na^+ transport ability vis-à-vis OsHKT1;5

Suji Somasundaram[1,8], Anne-Aliénor Véry[2,9], Rithvik S. Vinekar[3,8], Tetsuya Ishikawa[4], Kumkum Kumari[1,2], Shalini Pulipati[1], Kavitha Kumaresan[5], Claire Corratgé-Faillie[2], R. Sowdhamini[3], Ajay Parida[6], Lana Shabala[4], Sergey Shabala[4,7], Gayatri Venkataraman[1,8]

[1] Plant Molecular Biology Laboratory, M. S. Swaminathan Research Foundation, III Cross Street, Taramani Institutional Area, Chennai-600113, India

[2] Biochimie & Physiologie Moléculaire des Plantes, UMR Univ. Montpellier, CNRS, INRAE, SupAgro, , 34060 Montpellier Cedex 2, France

[3] National Centre for Biological Sciences, (TIFR), GKVK Campus, Bellary Road, Bangalore 560 065

[4] Tasmanian Institute of Agriculture, College of Science and Engineering, University of Tasmania, Private Bag 98, Hobart, Tas 7001, Australia

[5] Krishi Vigyan Kendra, Thurupathisaram, Kanyakumari District., Tamil Nadu, India-629901

[6] Institute of Life Sciences (ILS), NALCO Square, Bhubaneswar- 751023, Odisha, India

[7] International Research Centre for Environmental Membrane Biology, Foshan University, Foshan 528000, China

[9] authors have contributed equally to this study.

[8] Corresponding author

Abstract

HKT1;5 loci/alleles are important determinants of crop salinity tolerance. *HKT1*;5s encode plasmalemma-localized Na^+-transporters, retrieving xylem Na^+ into xylem parenchyma cells, reducing shoot Na^+ accumulation. Allelic variation in rice *OsHKT1*;5 sequence in specific landraces (Nona Bokra *OsHKT1;5-NB*/Nipponbare *OsHKT1;5-Ni*) correlates with variation in salt tolerance. *Oryza coarctata*, a halophytic wild rice, grows in fluctuating salinity at the seawater-estuarine interface in Indian and Bangladeshi coastal regions. The distinct transport characteristics of the shoots and roots expressing *O. coarctata* OcHKT1;5 transporter, are reported *vis-à-vis* OsHKT1;5-Ni. Yeast sodium extrusion-deficient cells expressing OcHKT1*;5* are sensitive to increasing Na^+ (10-100 mM). Electrophysiological measurements in *Xenopus* oocytes expressing *O. coarctata* or rice HKT1;5 transporters indicates that OcHKT1;5, like OsHKT1;5-Ni is a Na^+-selective transporter, but displays 16-fold lower affinity for Na^+ and 3.5-fold higher maximal conductance than OsHKT1;5-Ni. For Na^+ concentrations greater than 10 mM, OcHKT1;5 conductance is higher than that of OsHKT1;5-Ni, indicating potential of OcHKT1;5 for increasing domesticated rice salt tolerance. Homology modeling/ simulation suggests that four key amino acid changes in OcHKT1;5 (in loops on the extracellular side; E239K, G207R, G214R, L363V), account for its lower affinity and higher Na^+ conductance *vis-à-vis* OsHKT1;5-Ni. Of these, E239K in OcHKT1;5, confers lower affinity for Na^+ transport, as evidenced by Na^+ transport assays of reciprocal site directed mutants for both transporters (OcHKT1;5- K239E, OsHKT1;5-Ni-E270K) in *Xenopus* oocytes. Both transporters have analogous roles in xylem sap desalinization and differences in Na^+ transport affinity/ conductance between the transporters is attributable to differences in xylem sap Na^+ concentrations in both species.

Keywords: Halophyte, HKT1;5, homology modeling, Na^+ transporter, *Oryza coarctata*, simulation, *Xenopus* oocytes, yeast.

Introduction

Salinization affects lands that receive little rain or increased saline water input, attributable to natural as well as anthropogenic causes (Yang *et al.,* 2014). Saline soils negatively affect crop yield due to osmotic stress and cytotoxic effect of elevated cellular Na^+ and Cl^- concentrations, leading to inhibition of cell expansion, photosynthetic activity, enhanced leaf senescence and reductions in assimilate allocation to reproductive structures (Mickelbart *et al.,* 2015). Conserved salt tolerance mechanisms exist that control net Na^+ transport across the plasma membrane (HKT transporters/SOS1 antiporter), and/or tonoplast (NHXs antiporters) in both root and shoot, minimizing (with more or less efficacy), cytosolic and organellar Na^+ toxicity by ensuring maintenance of K^+/Na^+ homeostasis and facilitating vacuolar osmotic adjustment for turgor maintenance (Berthomieu *et al.,* 2003; Ren *et al.,* 2005; Bassil *et al.,* 2012; Oh *et al.,* 2009).

Increasing evidence suggests that *HKT1;5* loci and/or alleles are causal determinants for crop cereal tolerance in the field. HKT1;5 is a plasma membrane transporter that retrieves Na^+ from root xylem vessels (loaded/transferred to adjacent parenchyma cells), thus reducing xylem sap Na^+, minimizing shoot Na^+ transpirational flux, improving shoot K^+/Na^+ ratio. Introgression of the *Nax2* locus (containing *TmHKT1;5-A*) from wild wheat (*Triticum monococcum*) into commercial (salt sensitive) durum wheat (lacking *HKT1;5-A*) leads to significant reductions in leaf Na^+ concentration and enhanced grain yield on saline soils (Munns *et al.,* 2012). Salt tolerance of hexaploid bread wheat (AABBDD) is linked to the *KNA1* locus (harbouring *TaHKT1;5-D* contributed by parent *A. tauschii*) with subsequent neo-functionalization of *TaHKT1;5-D* conferring salt stress-induced expression (Yang *et al.,* 2014). RNAi silencing of *TaHKT1;5-D* in transgenic bread wheat leads to leaf Na^+ accumulation (Byrt *et al.,* 2014). TmHKT1;5-A has 2.8 fold higher affinity for Na^+ compared to TaHKT1;5-D, attributable to two specific changes: [$D^{471\ (TmHKT1;5\text{-}A)}$/no residue$^{(TaHKT1;5\text{-}D)}$] and [$D^{474\ (TmHKT1;5\text{-}A)}$/ $G^{473\ (TaHKT1;5\text{-}D)}$] (Xu *et al.,* 2018). In maize, two SNPs in the coding region of *ZmHKT1*;5 are significantly associated with variations in salt tolerance (Jiang *et al.,* 2018).

In rice, distinctions in salt tolerance of a set of landraces is connected with allelic variation in *OsHKT1;5* at the *Saltol* locus (Ren *et al.,* 2005; Thomson *et al.,* 2010). Further, higher root-specific expression of *OsHKT1;5* correlates with higher salt tolerance in a number of landraces (Cotsaftis *et al.,* 2012) and rice landraces that efficiently maintain shoot K^+/Na^+ homeostasis also display specific amino acid variation(s) in OsHKT1;5 sequence (Cotsaftis *et*

al., 2012; Negrão *et al.,* 2013; Platten *et al.,* 2013). A higher conductance of OsHKT1;5 transporter from the Nona Bokra salt tolerant variety has been reported as compared with the corresponding transporter from the salt sensitive Koshihikari (displaying four amino acid differences; Ren *et al.,* 2005). The impact of the allelic variation of OsHKT1;5 sequence on transporter performance however mostly remains to be determined.

Wild rice species are sources of gene diversity and have been used to increase domesticated rice yield, quality, resistance to diseases/ insects and tolerance to abiotic stress (Jena, 2010). *O. coarctata* (= *Porteresia coarctata*) is an allotetraploid halophytic wild rice species, found growing as a mangrove associate in the coastal regions of India and Bangladesh (Sengupta *et al.,* 2010; Jagtap *et al.,* 2006). Tidal/semi-tidal diurnal inundation of saline river or seawater in the inter-tidal region exposes *O. coarctata* to constantly fluctuating salinity, varying between 20-40 dS m^{-1} (Bal *et al.,* 1986). *O. coarcata* has evolved numerous mechanisms to deal with salinity as well as submergence. Salt glands on the leaf surface secrete Na^+, maintaining a low leaf Na^+/K^+ ratio even under high salinity (Flowers *et al.,* 1990). Aerenchymatous roots develop from extensively branching rhizomatous pseudo-taproots, anchoring it firmly to the soil even under inundated conditions (Latha *et al.,* 2004). *O. coarctata* demonstrates increased photosynthesis, better root and shoot growth, increased leaf biomass, higher relative water content in saline soils (Sengupta *et al.,* 2010).

With a view to achieving higher salinity tolerance, the objective of the present study was to examine the transport properties of wild rice *O. coarctata* HKT1;5 (OcHKT1;5) *vis-a-vis* cultivated rice OsHKT1;5-Ni in yeast and *Xenopus* oocyte expression systems. Subcellular localization and tissue specific expression of *HKT1*;5 in *O. coarctata* under salinity stress is examined. Finally, through homology modeling and simulation, a critical amino acid residue that distinguishes Na^+ transport properties of OcHKT1;5 *vis-à-vis* OsHKT1;5-Ni is identified and validated by transport assays of reciprocal site directed mutants for both transporters in *Xenopus* oocytes.

Results

Identification of a HKT1;5-type plasma membrane transporter from the halophytic wild rice *Oryza coarctata*

A *HKT1;5*-type cDNA was isolated from salt stressed roots of *Oryza coarctata* (Accession No: KU994892). The *OcHKT1;5* cDNA is 1,752 bp in length with 5` and 3` UTRs that are 41 bp and 136 bp in length respectively, and codes for an ORF of 521 amino acids. BLAST

analysis revealed that OcHKT1;5 polypeptide was more similar to *Oryza brachyantha* HKT1;5 (ObHKT1;5; 82% identity) compared to *Oryza sativa* OsHKT1;5 (79% identity). OcHKT1;5 was also 33 amino acids shorter than its rice homologues from Nipponbare (OsHKT1;5-Ni) or Nona Bokra (OsHKT1;5-NB). OcHKT1;5 clusters with other type 1;5 HKTs from wheat and rice (Fig. 1A).

OcHKT1;5 expression in *O. coarctata*

The tissue-specific expression pattern of *OcHKT1;5* in leaf and root tissues under standard growth conditions and salinity treatment was investigated (Fig. 1B-D). In absence of salt stress, *OcHKT1*;*5* was more expressed in roots than in shoots (Fig. 1B). Upon 150 mM NaCl treatment, *OcHKT1;5* expression in roots was increased 4-fold after 24 h of salt application, then downregulated significantly after 36-48h of salt application and remained downregulated after 48h of salt withdrawal (Fig. 1C). *OcHKT1*;5 expression in leaves was relatively un-altered by the salt treatment (Fig. 1D). A slight increase in expression (1.3 fold) was observed after 48 hours. The expression in leaf returned to initial level after salt withdrawal.

Sodium extrusion deficient yeast cells expressing OcHKT1;5 show sodium sensitivity

The Na^+ transporting ability of OcHKT1;5 was examined in yeast B31 cells (lacking Na^+ efflux mechanisms) in the presence of increasing NaCl concentrations. Growth inhibition of OcHKT1;5 transformed yeast cells was detectable from 10 mM Na^+ (Fig. 2A) in the plates and was marked at 50-100 mM NaCl relative to wild type or pYES2 transformed mutant B31 cells. Since inhibition was manifest at 50-100 mM NaCl, growth of OcHKT1;5 transformed yeast cells were examined for growth sensitivity in liquid cultures at the mentioned concentrations for shorter time periods. Yeast transformed with pYES:OcHKT1;5 grew slightly slower in 50 mM NaCl but their growth was almost abolished (85% inhibition) in 100 mM NaCl (Fig. 2B). All strains grew equally well in liquid media lacking supplemental NaCl (Fig. 2B). The results are consistent with a reduction in growth of yeast by OcHKT1;5 due to inward Na^+ transport.

OcHKT1;5 shows distinct sodium transport characteristics in *Xenopus* oocytes compared to OsHKT1;5-Ni

Further analysis of OcHKT1;5 functional properties were performed by two-electrode voltage clamp, after expression of the transporter in *Xenopus* oocytes. The rice homologue OsHKT1;5-Ni, was also expressed for comparison. In addition, control oocytes were injected

with water. The Na^+/K^+ selectivity of the transporters was addressed by comparing currents through the transporters in bath solutions containing combinations of two concentrations of Na^+ and K^+, 0.3 and 10 mM. Both transporters were well expressed in the *Xenopus* oocytes, mediating exogenous currents >10 times those of control oocytes in all used ionic conditions (Fig. 2C-E). Upon increase in external Na^+ concentration from 0.3 to 10 mM, OcHKT1;5 and OsHKT1;5-Ni current-voltage (I-V) relationships were positively shifted, and the inward conductance of the transporters at the whole oocyte level (slope of the relation between inward current and voltage) was increased (Fig. 2D and 2E respectively), indicating permeability to Na^+. Conversely, the reciprocal increase in external K^+ concentration from 0.3 to 10 mM did not have any effect on OcHKT1;5 and OsHKT1;5-Ni currents (Fig. 2D and 2E respectively), indicating (i) no significant permeability to K^+ and also (ii) no inhibitory effect of K^+ on activity of both transporters.

A detailed comparison of Na^+ transport by *O. coarctata* and rice HKT1;5 transporters was performed by analysing the two transporters in parallel in a set of bath solutions containing varying Na^+ concentrations from 0.03 to 100 mM (Fig. 3). Upon increase in external Na^+ concentration, the reversal potential of currents through the two transporters (E_{rev}) was similarly shifted (Fig. 3A-C). E_{rev} varied linearly with the logarithm of the external Na^+ activity in the range of 3 to 100 mM with a slope of 52 mV per decade of activity in OcHKT1;5 and 51 mV per decade of activity in OsHKT1;5-Ni. These experiments thus confirmed the high Na^+ selectivity of both transporters (variation of 58 mV per decade of activity expected in a purely selective Na^+ transporter). The evolution of inward conductance upon increase in external Na^+ concentration was also compared between the two transporters. Interestingly, hyperbolic function fit to the inward conductances highlighted strong differences between the two transporters in their apparent affinity for Na^+ (K_M = 32 mM in OcHKT1;5 *versus* 2 mM in OsHKT1;5-Ni) and in their maximal conductance (>3.5 times higher in OcHKT1;5) (Fig. 3D).

Homology modeling and simulation identifies key amino acid residues in OcHKT1;5 that govern Na^+ entry into the transporter

Homology modelling suggests that OcHKT1;5 has a pseudo-symmetric four-domain repeat structure D1-D4 (Supplementary Fig. S1). Each domain has a filter region (denoted by Fil#; Supplementary Fig. S2), which contributes one residue to the sodium selectivity filter, S_1-G_2-G_3-G_4 (Horie *et al.,* 2001), where S is serine and G is glycine. In bacterial potassium transporters, the corresponding G_1-G_2-G_3-G_4 motif of the selectivity filter allows K^+-

permeability. The distance between the main chain C-alpha atoms of S_1/G_1 and G_3 is thought to determine Na^+ specificity, as Na^+ has an ionic radius of 1.16 Å while K^+ has a radius of 1.52 Å. The presence of a sidechain in serine S_1 constricts the pore opening. Thus, the transporter pore completely excludes the larger ion, allowing only the smaller one to pass. OsHKT1;5-NB and OsHKT1;5-Ni differ from each other in four amino acid residues (OsHKT1;5-NB→OsHKT1;5-Ni): A140P, H184R, D332H and V395L (Supplementary Table S2, Supplementary Fig. S2). Of these, the V395L is thought to account for lower transport rates in OsHKT1;5-Ni (Cotsaftis *et al.,* 2012) and is V363 in OcHKT1;5, similar to OsHKT1;5-NB

Electrostatic interactions in the OsHKT1;5-Ni and OcHKT1;5 models were mapped (Fig. 4A and 4B)**.** Red areas denote negative charge while blue areas indicate positive charge. Both pore entrances are visible and are predominantly negatively charged. Key residue changes are highlighted. In domains D1, D2, and D3, key glutamate and aspartate residues E81, E83 (D1: conserved in OsHKT1;5-Ni, OsHKT1;5-NB and OcHKT1;5), E270 (D2: OsHKT1;5-Ni, OsHKT1;5-NB) and D366 (D3: OsHKT1;5-Ni, OsHKT1;5-NB; D334 in OcHKT1;5) provide an overall negative charge, favouring ion entry into the pore. In OcHKT1;5, the D2 glutamate is replaced by lysine (K239), a positively charged residue, less favorable for Na^+ entry. Further, the negative side chain of E270 in OsHKT1;5-Ni and OsHKT1;5-NB is positioned facing the positive charge provided by Lys244, the latter being flanked by two glycine residues (GKG) (Fig. 4C). In OcHKT1;5, the corresponding lysine, K213, is followed by R214 instead of glycine (Fig. 4D). Both K213 and R214 in OcHKT1;5 provide a strong positive environment, which will serve to repel K239 (Fig. 4F).

The 50 ns simulation of OcHKT1;5 and OsHKT1;5-Ni shows differences in the position of the charged residues at the pore entrance. In the OsHKT1;5 model, the acidic residues E81, E270 and D366 form a triad around the mouth of the transporter pore and mutually repel each other, keeping the entrance to the transporter pore open (Fig.4C-F). Distance plots demonstrating this are shown in Fig. 5A, 5B for the two simulations at 10 mM and 20 mM NaCl for 50 ns each. The G243-K-G245 loop in OsHKT1;5-Ni plays a minor role attracting E_{270} and E_{83}, causing the distance between E270-E81 to lessen compared to E270-D366, as seen in the 10 mM distance plot in Fig. 5A.

In OcHKT1;5, the corresponding triad residues are E81, K239 and D334. The E270 →K239 (OsHKT1;5-Ni → OcHKT1;5) change switches an acidic residue with a large basic

one. The K239 residue forms a salt bridge with D334, and sometimes can also form a salt bridge with E81 (Fig. 5C, 5D). These links can be released momentarily in the presence of Na^+ (Fig. 5C, D). The loop containing E81 has another acidic residue, E83. This seems to attract R214, causing the G212-K-R214 loop to move towards it. In doing so, the K213 residue further repels K239. This electrostatic repulsion serves to provide a bias towards the K239-D334 salt bridge, as opposed to the K239-D81 salt bridge (Figs 4E, F and 5C, D). Formation of the salt bridge is additionally biased by the positive charge introduced due to the G238→R207 residue change (OsHKT1;5-Ni → OcHKT1;5) (Fig. 4A, B).

Mutagenesis confirms the strong impact of E270K/K239E reciprocal amino acid residue changes in conferring the difference in HKT1;5 affinity for Na^+ and maximal conductance in *O. sativa* OsHKT1;5-Ni and *O. coarctata* OcHKT1;5

Site-directed mutagenesis was performed on *OsHKT1;5-Ni* and *OcHKT1;5* sequences to produce reciprocal mutations E270K (OsHKT1;5-Ni- E270K) and , K239E (OcHKT1;5-K239E) respectively on the translated transporter sequences. Both mutants were expressed in same batches of *Xenopus* oocytes along with wild type transporter *OsHKT1;5-Ni* as control, using identical amount of injected cRNAs. Na^+ currents through the different transporters were measured (in parallel on oocytes expressing the different clones; Fig. 6) in a set of bath solutions containing varying Na^+ concentrations (as above for the characterization of wild type transporters). The inward conductance of mutant and wild type transporter populations at the oocyte membrane was determined in different solutions for comparison of transport capacity between transporters (Fig. 6). Both mutations did not modify the transporter selectivity for Na^+ but strongly impacted the apparent affinity for Na^+ transport and maximal ion transport ability. E270K mutation in OsHKT1;5-Ni decreased the transporter affinity for Na^+ (3-fold increase in the K_M value) and increased the maximal conductance (by 52%) (Fig. 6E). The reciprocal mutation K239E in OcHKT1;5 had the opposite effect: increase in transporter affinity for Na^+ (9-fold decrease in the K_M value), and decrease in the maximal conductance (by 48%) (Fig. 6F).

Xylem sap estimation in *O. coarctata* and *O. sativa* L. (*cv.* Koshihikari)

Under control conditions, xylem sap Na^+ concentration of *O. coarctata* was ~3 mM and significantly higher than in *O. sativa* ($P< 0.05$). Salinity exposure (80 mM NaCl for one week) resulted in a 5-fold increase in its value in wild rice (Fig. 7A). In *O. sativa,* however,

xylem sap Na^+ concentration at this point reached ~ 65 mM, a 100-fold increase compared with *O. sativa* under control conditions (both changes significant at $P< 0.001$; Fig. 7A). Xylem sap K^+ concentrations in the two species under control conditions did not show a significant difference, but salinity treatment significantly ($P< 0.05$) increased xylem sap K^+ in *O. sativa* compared with *O. coarctata* (Fig. 7B).

Discussion

Allelic differences in the rice *HKT1;5* ORF (four non-synonymous nucleotide substitutions) have been noted between salt tolerant (Nona Bokra) and sensitive (Koshihikari) rice landraces (Ren et ., 2005). Seven major and three minor alleles of *OsHKT1*;5 have been identified in *O. sativa* landraces, with the '*Aromatic'* allele (present in Nona Bokra) showing a very strong correlation with shoot Na^+ exclusion (Platten *et al.,* 2013). However, HKT1;5 diversity has not been examined in wild rice species so far. *Oryza coarctata* is the only species among wild rice that is highly adapted to salinity as well as submergence tolerance. It is found growing in coastal regions of India and Bangladesh, where it experiences semi-tidal inundation with saline seawater (Menguer *et al.,* 2017). We therefore chose *O. coarctata*, a salinity tolerant wild rice, for examining HKT1;5 activity.

OcHKT1;5 encodes a salinity inducible sodium transporter

OcHKT1;5 codes for a 521 amino acid protein that localizes to the plasma membrane (Supplementary Figure S3) and shows high similarity with *Oryza brachyantha* HKT1;5 and OsHKT1;5 (Fig. 1A). Under low saline conditions, expression of *OcHKT1*;5 in roots is higher than in leaves (Fig. 1B). *OcHKT1;5* expression in roots is upregulated only at 24h of salt application. At all other time points of salinity application examined, *OcHKT1;5* expression in root is lower than in leaves (Fig. 1, B-D) and contrasts with *OsHKT1*;5 expression in rice under salinity. Ren *et al.,* (2005) have reported a root specific upregulation of *OsHKT1;5* expression (*OsHKT1;5* is preferentially expressed in the xylem parenchyma cells of roots). Further, rice landraces showing higher root expression of *OcHKT1*;5 show higher shoot Na^+ exclusion (Cotsaftis *et al.,* 2012). In wheat and barley too, under salinity, HKT1;5 genes show root-specific expression (Byrt *et al.,* 2007; Hazzouri *et al.,* 2018). Thus, substantial expression of *OcHKT1;5* in leaves (higher than roots following salinity treatment) contrasts with the expression profile of *HKT1;5*-type genes in other species. This may be related to a specific mechanism of adaptation to high salinity in *O. coarctata*.

OcHKT1;5 shows higher Na^+ transport capacity than the rice OsHKT1;5-Ni at high Na^+ concentrations

Analysis of expression of OcHKT1;5 in sodium extrusion deficient yeast B31 cells and electrophysiological data show that OcHKT1;5 is a Na^+-selective transporter (Fig. 2D), like other HKT1;5-type systems characterized in rice and wheat species (Ren *et al.,* 2005; Munns *et al.,* 2012; Byrt *et al.,* 2014). In contrast to ion selectivity, Na^+ transport affinity is highly variable within the members of the HKT subfamily 1. Thus, while OsHKT1;5-Ni in rice (Fig. 3D) and TmHKT1;5-A in wheat display highest Na^+ transport affinity values [$K_{M\ (oocytes)} \leq 2$ mM Na^+), OsHKT1;1 displays very low transport affinity when expressed in yeast or oocytes [$K_{M\ (oocytes)} \sim 75$ mM Na^+) and OsHKT1;3 a 20 times higher affinity ($K_M \sim 3.5$ mM Na^+) than OsHKT1;1 (Garciadeblás *et al.*, 2003; Jabnoune *et al.,* 2009; Munns *et al.,* 2012). OcHKT1;5 Na^+ transport affinity is very low as compared to other HKT1;5-type transporters: ~8 to 35 times lower than for OsHKT1;5-Ni and the wheat TmHKT1;5-A and TaHKT1;5-D (Fig. 3D; Munns *et al.,* 2012; Byrt *et al.,* 2014; Xu *et al.,* 2018).

Interestingly, functional differences were reported as likely basis of several salt tolerance QTLs involving *HKT* genes (Ren *et al.,* 2005; Tounsi *et al.,* 2016; Campbell *et al.,* 2017). Among these differences, important variabilities in Na^+ transport affinity and/or maximal conductance were found: TmHKT1;4-A2 from *T. monococcum*, seemingly responsible for salt tolerance improvement of durum wheat within the *Nax2* QTL displays (when expressed in *Xenopus* oocytes) 3-11 times lower Na^+ transport affinity and 2-4 times higher maximal conductance than its durum wheat TdHKT1;4-1 and TdHKT1;4-2 homologues (Ben Amar *et al.,* 2014; Tounsi *et al.,* 2016). Thus, at Na^+ concentrations >10 mM, TmHKT1;4-A2 is more efficient at transporting Na^+ than its durum wheat homologues (Tounsi *et al.,* 2016). TmHKT1;5-A has 2.8 fold higher affinity for Na^+ ($K_M \sim 2.7$ mM) compared to TaHKT1;5-D ($K_M = 7.5$ mM; Xu et al., 2018). In rice, The *SKC1* QTL was also proposed to be explained by differences in Na^+ transport ability between OsHKT1;5-NB from the salt tolerant variety Nona Bokra and its homologue from the salt sensitive variety Koshihikari (Ren et al., 2005). No significant difference in expression between the two variants was observed. Therefore, the 50% higher conductance of the Nona Bokra OsHKT1;5 transporter, highlighted by transport assays in *Xenopus* oocytes, is likely to underlie the functional difference between the two alleles *in planta* (Ren *et al.,* 2005).

In the present study, Nipponbare, was chosen as a salt sensitive rice control. OsHKT1;5-Ni sequence is identical to Koshihikari OsHKT1;5 (Cotsaftis *et al.,* 2012). When expressed in *Xenopus* oocytes, *O. coarctata* OcHKT1;5 displays a 16-fold lower Na^+ transport affinity and 3.5-fold higher maximal conductance than OsHKT1;5-Ni (Fig. 3D) which may be due to higher unitary transporter conductance or higher number of transporters at the membrane. This leads to higher conductance for OcHKT1;5 at Na^+ concentrations ≥ 10 mM, by ∼100% at 30 mM Na^+ and ∼200% at 100 mM Na^+ (Fig. 3D). Thus, OcHKT1;5 appears more efficient at transporting Na^+ than OsHKT1;5-Ni in high salinity conditions.

Homology modeling identifies critical amino acid residues in OcHKT1;5 that contribute to its lower Na^+ affinity

While OcHKT1;5 shows sodium specific transport, consistent with the presence of the S-G-G-G pore motif (Mäser *et al.,* 2002), its affinity for Na^+ is several folds lower than OsHKT1;5-Ni. Two factors appear to likely contribute to OcHKT1;5 lowered affinity: (i) lowering of the overall negative charge at the ion pore entrance of OcHKT1;5 due to the presence of a positively charged residue, K239 (E270 in OsHKT1;5-Ni/OsHKT1;5-NB; Fig. 4) and (ii) narrowing of the ion pore entrance in OcHKT1;5 due to attraction between D334 and K239 (reinforced by repulsion between K239 and the positively charged K213, R214 residues in the second pore domain). K239 placed over the pore entrance, provides steric hindrance as well as an unfavorable electrostatic environment for an approaching cation. Simulation shows that there are occasions where the K239-D314 distance increases with a corresponding decrease in the K239-E81 distance, but is restored back. Sodium ions approaching the transporter seem to trigger such changes, albeit temporarily (Fig. 5). Approaching cations affect the local environment, and a sufficiently large enough cation concentration may displace K239 from its position, restoring activity. The strong impact of the E *vs* K residue at the 270/239 position in the rice and *O. coarctata* HKT1;5 transporters respectively was confirmed by functional characterization after reciprocal residue exchange. As predicted by modelling, the lowering of the overall negative charge at the pore entrance of OsHKT1;5-Ni by E270K change decreased the transporter affinity for Na^+ by three-fold, and the reciprocal increase in negative charge at the respective position in OcHKT1;5 by K239E change increased Na^+ transport affinity by almost 9-fold (Fig. 6). The maximal conductance of OcHKT1;5 was also impacted by this K to E change, coming closer to that of OsHKT1;5-Ni (Fig. 6). Of the 27 amino acid residue differences between TmHKT1;5A and TaHKT1;5D, six residue substitutions are predicted to be significant through 3D modeling

(Xu *et al.*, 2018). Among the six residues, D471 and D474 from TmHKT1;5-A occur very close to each other and form a part of an α-helix which directly links to one of the loops forming the selectivity filter . The former has no counterpart in TaHKT1;5D while the latter is substituted by G473. Reciprocal double mutations reduce Na^+ affinity of TmHKT1;5A (K_M = 3.9 mM) and increase Na^+ affinity of TaHKT1;5D (K_M = 4.1 mM) to similar levels. These changes had lower impact on transporter conductance (1.5-2 fold change) than the E/K reciprocal changes that we experimentally show here in the rice/*O. coarctata* HKT1;5 transporters (3-9 fold changes, Fig. 6).

OsHKT1;5-NB and OsHKT1;5-Ni differ from each other in four amino acid residues. Of these, V395L is thought to account for lower transport rates in OsHKT1;5-Ni (Cotsaftis et al*.,* 2012). The V395L substituted residue in OsHKT1;5-Ni is positioned strategically in the close proximity of Gly391 (G3 filter residue) near the entrance of the pore (of both OsHKT1;5-NB and OsHKT1;5-Ni; Fig. 4A, B; Supplementary Fig. S1). The V395L replacement changes the geometry of the filter loop, possibly decreasing the distance between S_1 and G_3 at the S_1-G_2-G_3-G_4 position, thus being unfavorable for ion entry. The larger side-chain of V395 as compared to L395 causes the loop with G_3 to shift, further constricting the pore. It could also directly affect pore rigidity, due to a larger van der Waals volume imposed by the side-chain of L395 compared to that of V395 and thus slow down Na^+ transport rates. The V395L substitution in Ni-OsHKT1;5 could also influence the dispositions of other key residues underlying the Na^+ transport within the pore environment. In the OcHKT1;5 polypeptide, OsHKT1;5-NB V395 is conserved as V363. Valine also appears to be present in TaHKT1;5D, TmHKT1;5A, barley and maize HKT1;5 sequences (Su *et al.,* 2015). The higher maximal conductance of OcHKT1;5 as compared to OsHKT1;5-Ni is in agreement with the previous hypothesis of a key role of V *versus* L at this position in promoting high rates of Na^+ transport.

Physiological relevance of OcHKT1;5 transport features in relation to xylem sap Na^+ concentration under salinity

O. coarctata plants maintain low Na^+/K^+ ratios even after six weeks of growth in artificial sea water (25 % ASW). This is in part due to sodium secretion by microhairs on the adaxial leaf surface under salinity (Flowers *et al.,* 1990). We show here that this is also due to a control of the concentration of Na^+ arriving to the shoots through the xylem sap (Fig. 7A). Maintenance of cytosolic Na^+ concentration below toxic levels is important for salinity stress tolerance,

and control of xylem Na^+ loading is often considered as one of the most crucial characteristics for salinity tolerance (Munns and Tester, 2008). Salt-sensitive rice cultivar (*O. sativa*) fails to control xylem Na^+ loading while salt-tolerant *O. coarctata* has an initially higher level of Na^+ in the xylem (under non-saline conditions) but is able to prevent its drastic increase under saline conditions (Fig. 7A). The initial high xylem sap Na^+ concentration of *O. coarctata* can be explained as a typical trait of halophytes in that they require a high level of salt for optimal growth (Shabala, 2013), thus actively absorbing Na^+ under non-saline conditions. Salt-sensitive Koshihikari relies more on an increase in xylem K^+ loading in response to salinity compared with *O. coarctata* (Fig. 7B), partly in compensation for increased xylem Na^+ concentration, to maintain K^+/ Na^+ homeostasis. Halophytic species and salt tolerant glycophytes genotypes can reduce the amount of xylem Na^+ loading and increase Na^+ retrieval back from xylem, thus maintaining a normal plant growth under salinity conditions (Zarei *et al.,* 2019, Ishikawa and Shabala, 2019).

We propose that OcHKT1;5 has an analogous role to OsHKT1;5-Ni in xylem sap desalinization (Ren et al., 2005; Kobayashi et al., 2017). Differences in Na^+ transport affinity and maximal conductance between the two transporters (Fig. 3) relate to the differences in the xylem sap Na^+ concentrations observed in the two species. In low salt conditions, OsHKT1;5 (Koshihikari and Nipponbare variants being identical) which displays higher affinity than OcHKT1;5 would be more conductive (Fig. 3D) and, if similarly expressed, thus more efficient at xylem sap desalinization, resulting in the observed lower xylem sap Na^+ concentration in *O. sativa* compared to *O. coarctata* plants (Fig. 7A). In contrast, in high salinity conditions, the lower affinity and higher conductance of the *O. coarctata* transporter (Fig. 3D) would make it more efficient for xylem sap desalinization than its rice homologue, explaining the lower xylem sap Na^+ concentration in *O. coarctata* compared to *O. sativa* plants in these conditions (Fig. 7A). The Na^+ concentrations measured in xylem sap under salinity treatment (higher than 15 mM) are compatible with this hypothesis (Fig.3D, Fig. 7A). This transport in *O. coarctata* therefore, is sufficient to use Na^+ as a cheap osmoticum and maintain shoot cell turgor and, hence, its growth under hyperosmotic saline conditions.

Thus, owing to its almost linear increase in conductance up to concentrations higher than 100 mM, OcHKT1;5, may control a relatively stable Na^+ concentration in xylem sap. Below a certain 'threshold' of cellular Na^+, it would trigger little Na^+ sequestration into

xylem parenchyma. With increase in Na^+ concentrations secreted to the xylem sap, OcHKT1;5-mediated Na^+ transport (and Na^+ sequestration) would increase, limiting change in the amount of Na^+ transported to the shoots. Growing in a habitat with real time fluctuations in salinity, OcHKT1;5 transport properties may have evolved uniquely with xylem parenchyma sequestration of Na^+ being tuned to Na^+ sap concentration so that 'toxic' Na^+ levels are not built up in the plant.

Methods

Cloning of *OcHKT1;5* cDNA

O. coarctata tillers with intact roots were subjected to 0.25 M NaCl (12h, 24h). Total RNA was isolated from salinity treated roots of *O. coarctata*. *O. coarctata* genomic sequence information was used to design primers to isolate the *OcHKT1*;5 cDNA as two overlapping fragments by RT-PCR (5` *OcHKT1;5*-RT fragment: 1.1 Kb and 3` *OcHKT1;5*-RT fragment:700 bp) using *OcHKT1*;5 specific primers (5` OcHKT1;5 RT fragment: PcHKT RT FWD3/OsHKT8 REV1 and 3` OcHKT1;5 RT fragment:OsHKT8 FWD2/PcHKT1;5 RT REV; Supplementary Table S1). The two overlapping fragments were assembled together by SOE-PCR, cloned (T-vector; MBI Fermentas) and sequenced completely to check for ORF integrity.

O. coarctata growth conditions

O. coarctata plantlets growing in the mangrove forests (estuarine region) of Pichavaram, Tamil Nadu, India were uprooted and maintained along with the associated soil in tap water for about one month at 28±5ºC in the greenhouse. After development of new roots and tillers plants were transferred to 0.5X Murashige Skoog medium (liquid; Murashige and Skoog, 1962) and acclimatized for 48 hours. For stress treatments, the tillers were transferred to 0.5X with 150 mM NaCl. Leaf and root tissues were frozen in liquid nitrogen at time points indicated [0h, 12h, 24h, 36h, 48h and 48h withdrawal (WD)] for total RNA isolation (Supplementary Methods M1).

qRT-PCR analysis of *OcHKT1;5* expression in *O. coarctata*

O. coarctata total RNA (leaf, root) was re-purified using QIAGEN RNeasy Mini Kit. cDNA synthesis was performed in a reaction volume of 20 µl with 5 µg of total RNA, BioScript Reverse Transcriptase (Bioline, USA) at 45º C (60`), followed by heat inactivation at 70º C

(10 min). Primer pairs OcHKT RT FWD1/OcHKT RT REV1 and ACTIN 1 FWD/ACTIN 1 REV (Supplementary Table S1) were used for qRT-PCR to amplify fragments of sizes 134 bp (OcHKT1;5) and 125 bp (*Ocβ-Actin*) respectively. SYBR Green RT-PCR assay was carried out using the Step One Plus ™ Real-time PCR system (Applied Biosystems, USA) using synthesized cDNA samples. Each real-time PCR reaction was performed in triplicates, in order to evaluate data reproducibility for two biological replicates. The specificity of the amplicons was verified by melting curve analysis (60 to 95 °C) after 40 cycles. *OcHKT1;5* expression levels were estimated in *O. coarctata* leaf and root tissues using $2^{-\Delta\Delta Ct}$ and the value represented as n-fold difference relative to the control (*Ocβ-Actin*).

Yeast expression and growth

Na^+ uptake tests were performed using the yeast strain B31 sensitive to Na^+ accumulation [lacking Na^+ efflux systems ENA1-4 and ΔNHA1; *MAT α ena1Δ::HIS3::ena4Δ nha1 Δ::LEU2*; Bañuelos *et al.,* 1998] . The *OcHKT1;5* ORF was cloned in *pYES2* and transformed into B31 strain (lithium acetate method). B31 cells transformed with pYES2 served as negative control. B31 cells transformed with pYES:OcHKT1;5/pYES2 were grown to an Abs_{600} = 0.6, pelleted and resuspended in AP-Gal medium. Wild type cells (W303.1) or B31 cells (transformed with pYES:OcHKT1;5/pYES2 were plated on AP-Gal medium containing adenine (20 mg/l), tryptophan (30 mg/l) and NaCl (0, 10, 25, 50 or 100 mM NaCl). Plates were incubated at 30ºC for 3-4 days and growth examined. The drop test was repeated thrice, each time with two replicates.

To examine growth in liquid cultures, 200 µl of fresh culture was inoculated in 5 ml AP-Gal, grown overnight with shaking (180 rpm) at 30ºC. An aliquot of the overnight culture was inoculated in 10 ml AP-Gal medium with adenine and tryptophan and increasing NaCl (0, 50 or 100 mM), so that the initial $Abs_{600}$was ~0.2. The cultures were incubated at 30ºC with shaking (180 rpm) and growth measured spectrophotometrically (UV-1601, Shimadzu, Japan) at 24 hours.

Functional characterization of Na^+ transporters expressed in *Xenopus* oocytes

The ORFs of *OcHKT1;5*, *OsHKT1;5-Ni* (Clone 002-148-F10: from cv Nipponbare; Rice Genome Resource Center, NIAS, Japan), and *OcHKT1;5* and *OsHKT1;5-Ni* mutants were subcloned into a modified pGEMHE vector (Lebaudy *et al.,* 2010). *OcHKT1;5*, *OsHKT1;5-Ni* ORFs cloned in pGEM-HE were modified by site-directed mutagenesis to generate

reciprocal mutants using the QuikChange Site-Directed Mutagenesis Kit (Stratagene, La Jolla, CA, USA). Forward and reverse primers used for mutagenizing OcHKT1;5 to OcHKT1;5-K239E are as follows (i) OcHKT1;5-K239EFwd: 5'-CTTCGTGCCGACGAAC**G**AGGGGATGATCTCGTTC-3', (ii) OcHKT1;5-K239ERev: 5'-GAACGAGATCATCCCCT**C**GTTCGTCGGCACGAAG-3'. Forward and reverse primers used for mutagenizing *OsHKT1;5-Ni* to *OsHKT1;5-Ni*-E270K are as follows (i) NiHKT E270K Fwd: 5'-GTGCCGACGAAC**A**AAGGGATGGTGTCGTT -3', (ii) NiHKT E270K Rev: 5'-GAACGACACCATCCCTT**T**GTTCGTCGGCAC-3'. Both mutated ORFs (OcHKT1;5-K239E; *OsHKT1;5-Ni*-E270K) were sequenced completely for validation of the mutation and verification of absence of other randomly introduced mutations.

Capped and polyadenylated cRNAs were synthesized *in vitro* using mMESSAGE mMACHINE T7 kit (Ambion) following manufacturer's instructions. Oocytes isolated as previously described (Véry *et al.,* 1995) were injected with *OcHKT1;5, OsHKT1;5-Ni* or mutant transporter cRNA (30 ng in 30 nl) or 30 nl of RNase-free water (control oocytes) and kept at 18°C in ND96 medium (Véry *et al.,*, 1995). Electrophysiological measurements on oocytes were made 1–2 days following the injection according to Mian *et al.* (2011). Perfusion solutions contained as background 6 mM $MgCl_2$, 1.8 mM $CaCl_2$ and 10 mM MES-1,3-bis[tris(hydroxymethyl) methylamino] propane, pH 5.5. Monovalent cations were added to the background as glutamate salts, with osmolarity of solutions adjusted (if necessary) using D-mannitol (220–240 mOsmol/l). Data acquisition and analysis was performed using pCLAMP10 (Axon Instruments) and Sigmaplot11 (Jadel Scientific) software. To extract OcHKT1;5-, OsHKT1;5-Ni- or reciprocal mutant transporters-mediated currents from total oocyte currents, mean currents recorded in water-injected control oocytes (from the same oocyte batch in the same ionic conditions) were subtracted from those recorded in the transporter-expressing oocytes. OcHKT1;5, OsHKT1;5-Ni and reciprocal mutant transporter current–voltage (I–V) relationships were constructed with transporter extracted currents.

Homology Modelling

The sequences of OcHKT1;5, OsHKT1;5-NB (Nona Bokra variant), and OsHKT1;5-Ni (Nipponbare variant) were aligned with the closest homologous structures available in the Protein Databank: bacterial potassium transporters KtrAB from *Bacillus subtilis* (PDB: 4J7C; Vieira-Pires *et al.,* 2013, subunits I,J; resolution 3.5Å) and TrkH from *Vibrio parahaemolyticus* (PDB:3PJZ; Cao *et al.,* 2011; resolution 3.51Å). The former has 17.6 %

identity with OsHKT1;5, while the latter has 14.8 % identity. 4J7C is used as the main template, while N-terminal and C-terminal parts not represented in 4J7C are derived from 3PJZ. The homology model by Cotsaftis *et al.,* (2012) utilized only the 3PJZ template. The alignment and the structural correspondence for each domain are shown in Supplementary Figures S1 and S2.

JPred (Drozdetskiy *et al.,* 2015) and PsiPred (Jones, 1999) were used to predict secondary structure in regions not aligned with the template. Possible formation of beta sheet between the two subunits have been added as restraints for modelling, due to alternating beta strands predicted with glycine residues present between them. The ions present in the pore allow additional restraints and were included as BLK or block residues in the modelling program MODELLER (Eswar *et al.,* 2007) to aid the modelling process. Each modeller run generated 100 models and 5 loop refinement runs per model. The DOPE score for the models were sorted and the lowest score model selected. The model was inspected for knots and aberrations, if found discarded, with the subsequent correct model chosen. Short runs of minimization were done in the MODELLER protocol. Further minimization was done before simulation by setting the protein in the lipid layer.

Simulation

The MEMBED (Wolf *et al.,* 2010) protocol was used from Gromacs (Abraham *et al.,* 2015) to embed the monomer of the homodimer model. The Gromos53a6 (Oostenbrink *et al.,* 2004) united-atom forcefield with the recommended SPC (Berweger *et al.,* 1995) water model was used for the protein and solvent. Pre-equilibrated Dipalmitoyl phosphocholine (DPPC) lipid coordinates with Berger Lipid parameters (Berger *et al.,* 1997) were used to create the membrane. Within the homodimer, subunit A of OsHKT1;5 and subunit B of OcHKT1;5 were chosen as these were better defined. The model was aligned with the transporter pore in the center along the Z-axis and the OPM/PPM server (Lomize *et al.,* 2012) was used to determine the position of the bilayer. Five systems were simulated with a total of 250 ns. OsHKT1;5 and OcHKT1;5 systems were generated for 10 mM and 20 mM NaCl concentrations. Periodic boundary conditions with Particle Mesh Ewald (PME) electrostatics were utilized. Approximately 143000 particles were present in each system, with 5000 protein and 23800 lipid particles.

Minimization was done followed by relaxation using restraints on the protein and the lipids, with subsequent runs to relax the lipids. Both these runs were done under constant number of particles (N), volume (V) and temperature (T), i.e. NVT conditions with temperature set at 310K. Finally, an equilibration run was done for 1 ns under constant number of particles (N), pressure (P) and temperature (T), i.e. NPT conditions allowing the volume to adjust anisometrically: separately along the x-y directions where lipids play a role, and along the z-direction where only water is present, in order to obtain a relaxed system. Care was taken to ensure that vacuum bubbles in the lipid region were removed and no solvent or ion had entered the lipid region. Simulation was run for 50 ns for each system, without the presence of external restraints, using the Langevin thermostat and piston (Schneider & Stoll, 1978).

Xylem sap estimation in *O. coarctata* and *O. sativa* L. (*cv.* Koshihikari)

Tillers of newly developed (three to four-leaf stage) *Oryza coarctata* and *Oryza sativa* cv. Koshihikari of the same physiological age (i.e. seven days after sowing pre-germinated seeds) were transferred to the hydroponic medium containing 0.5 strength Murashige Skoog media (Sigma M-5519). Plants were grown under controlled conditions (25 ℃, day/night 15/9 h; 55% relative humidity). The hydroponic solutions were replaced every three days. Five days after seedling transfer to hydroponic medium, plants were treated with 80 mM NaCl for 7 days and xylem sap was collected. Plant shoots were cut 20 mm from the rhizome (*O. coarctata*)/ root crown (*O. sativa cv.* Koshihikari) and inserted (cut surface up) into a Scholander pressure chamber (Plant Moisture System, Santa Barbara, CA). Compressed air was filled into the chamber for applying pressure (about 10 and 20 bars for control and 80 mM NaCl treatment, respectively) and extruded xylem sap was immediately collected using a micropipette. Collected samples were weighed to 0.1 mg accuracy and diluted with double distilled water to measure Na^+ and K^+ concentrations by flame photometry (PFP7, Jenway, Essex, UK).

Acknowledgements

We thank Dr. Alonso Rodriguez-Navarro (Universidad Politécnica de Madrid) for the yeast strain and acknowledge funding from Department of Biotechnology, Government of India (Project No: BT/PR11396/NDB/52/118/2008) to Gayatri Venkataraman (PI) and Kavitha Kumaresan (Co-PI). Gayatri Venkataraman also acknowledges financial support from the

Indo-Australian Biotechnology Fund (BT/Indo-Aus/09/03/2015) grant provided by the Department of Biotechnology, Government of India. Shalini Pulipati acknowledges the Council for Scientific and Industrial Research (CSIR) for Senior Research Fellowship (SRF) (File No: 09/656 (0018)/2016-EMR-1). Kumkum Kumari received a short term EMBO fellowship (STF-7507) to carry out part of this work in the laboratory of Anne-Aliénor Véry (Montpellier, France). Sergey Shabala acknowledges the financial support from Australia-India Strategic Research Fund (project AISRF48490) and China National Natural Science Foundation (project 31870249).

Authors' contributions

G.V.: Conceived and designed the study; S.S.: Yeast based assays, qRT-PCR, subcellular localization, A-A.V. K. K. (Kumkum Kumari) and C.C.F. *Xenopus* oocyte transport assays; R.S.V. and R.S.: Homology modeling and simulation; T.I., L.S., S.S.: xylem sap analysis; S.P.: site directed mutagenesis; K.K. (Kavitha Kumerasan) and G,V.: cDNA isolation and cloning. A.P., A.-A.V., R.S., L.S., S.S., G.V. analysis of data and manuscript development. All authors read and approved the final manuscript. All authors declare they have no professional, personal or financial conflicts of interest.

References

1. Abraham M.J., Murtola T., Schulz R., Páll S., Smith J.C., Hess B. & Lindahl E. (2015) GROMACS: High performance molecular simulations through multi-level parallelism from laptops to supercomputers. *SoftwareX*, **1**, 19-25.
2. Bañuelos M.A., Sychrová H., Bleykasten-Grosshans C., Souciet J.-L. & Potier S. (1998) The Nhal antiporter of *Saccharomyces cerevisiae* mediates sodium and potassium efflux. *Microbiology*, **144**, 2749-2758.
3. Bal A. & Dutt S. (1986) Mechanism of salt tolerance in wild rice (*Oryza coarctata* Roxb). *Plant and Soil*, **92**, 399-404.
4. Bassil E., Coku A. & Blumwald E. (2012) Cellular ion homeostasis: emerging roles of intracellular NHX Na^+/H^+ antiporters in plant growth and development. *Journal of Experimental Botany*, **63**, 5727-5740.
5. Ben Amar S., Brini F., Sentenac H., Masmoudi K. & Véry A.-A. (2013) Functional characterization in *Xenopus* oocytes of Na^+ transport systems from durum wheat reveals diversity among two HKT1;4 transporters. *Journal of Experimental Botany*, **65**, 213-222.
6. Berger O., Edholm O. & Jähnig F. (1997) Molecular dynamics simulations of a fluid bilayer of dipalmitoylphosphatidylcholine at full hydration, constant pressure, and constant temperature. *Biophysical Journal*, **72**, 2002-2013.
7. Berthomieu P., Conéjéro G., Nublat A., Brackenbury W.J., Lambert C., Savio …, Casse F (2003) Functional analysis of *AtHKT1* in *Arabidopsis* shows that Na^+ recirculation by the phloem is crucial for salt tolerance. *The EMBO Journal*, **22**, 2004-2014.
8. Byrt C.S., Platten J.D., Spielmeyer W., James R.A., Lagudah E.S., Dennis E.S., …, Munns R. (2007) HKT1; 5-like cation transporters linked to Na^+ exclusion loci in wheat, *Nax2* and *Kna1*. *Plant Physiology*, **143**, 1918-1928.
9. Byrt C.S, Xu B, Krishnan M, et al. (2014) The Na^+ transporter, *TaHKT1; 5-D*, limits shoot Na^+ accumulation in bread wheat. *The Plant Journal*, **80**, 516-526.
10. Campbell M.T., Bandillo N., Al Shiblawi F.R.A., Sharma S., Liu K., Du Q., …, Walia H. (2017) Allelic variants of *OsHKT1;1* underlie the divergence between *indica* and *japonica* subspecies of rice (*Oryza sativa*) for root sodium content. *Plos Genetics* **13**(6).

11. Cao Y., Jin X., Huang H., Derebe M.G., Levin E.J., Kabaleeswaran V., …, Weng J. (2011) Crystal structure of a potassium ion transporter, TrkH. *Nature*, **471**, 336-340.
12. Cotsaftis O., Plett D., Shirley N., Tester M. & Hrmova M. (2012) A two-staged model of Na^+ exclusion in rice explained by 3D modeling of HKT transporters and alternative splicing. *PLoS One*, **7**, e39865.
13. Drozdetskiy A., Cole C., Procter J. & Barton G.J. (2015) JPred4: a protein secondary structure prediction server. *Nucleic Acids Research*, **43**, W389-W394.
14. Edgar R.C. (2004) MUSCLE: a multiple sequence alignment method with reduced time and space complexity. *BMC Bioinformatics*, **5**, 113.
15. Flowers T., Flowers S., Hajibagheri M. & Yeo A. (1990) Salt tolerance in the halophytic wild rice, Porteresia coarctata Tateoka. *New Phytologist*, **114**, 675-684.
16. Garciadeblás B., Senn M.E., Bañuelos M.A. & Rodríguez-Navarro A. (2003) Sodium transport and HKT transporters: the rice model. *The Plant Journal* **34**, 788–801.
17. Henderson, S. W., Dunlevy, J. D., Wu, Y., Blackmore, D. H., Walker, R. R., Edwards, E. J., ... & Walker, A. R. (2018). Functional differences in transport properties of natural *HKT1;1* variants influence shoot Na^+ exclusion in grapevine rootstocks. *New Phytologist*, *217*(3), 1113-1127.
18. Horie T., Motoda J., Kubo M., Yang H., Yoda K., Horie R., …, Konomi M. (2005) Enhanced salt tolerance mediated by AtHKT1 transporter-induced Na^+ unloading from xylem vessels to xylem parenchyma cells. *The Plant Journal*, **44**, 928-938.
19. Horie T., Yoshida K., Nakayama H., Yamada K., Oiki S. & Shinmyo A. (2001) Two types of HKT transporters with different properties of Na^+ and K^+ transport in *Oryza sativa*. *The Plant Journal*, **27**, 129-138.
20. Huson D.H., Richter D.C., Rausch C., Dezulian T., Franz M. & Rupp R. (2007) Dendroscope: An interactive viewer for large phylogenetic trees. *BMCBioinformatics*, **8**, 460.
21. Ishikawa I., & Shabala S. (2019) Control of xylem Na^+ loading and transport to the shoot in rice and barley as a determinant of differential salinity stress tolerance. *Physiologia Plantarum,* **165,** 619-631.

22. Jabnoune M., Espeout S., Mieulet D., Fizames C., Verdeil J.-L., Conéjéro G., …, Véry A.-A. (2009) Diversity in expression patterns and functional properties in the rice HKT transporter family. *Plant Physiol*ogy **150**, 1955-1971.

23. Jagtap T.G., Bhosale S. & Charulata S. (2006) Characterization of *Porteresia coarctata* beds along the Goa coast, India. *Aquatic Botany*, **84**, 37-44.
24. Jiang, Z., Song, G., Shan, X., Wei, Z., Liu, Y., Jiang, C., ... & Li, Y. (2018). Association analysis and identification of *ZmHKT1*;5 variation with salt-stress tolerance. *Frontiers in Plant Science*, *9*.
25. Jones D.T. (1999) Protein secondary structure prediction based on position-specific scoring matrices. *Journal of Molecular Biology*, **292**, 195-202.
26. Kobayashi N.I., Yamaji N., Yamamoto H., Okubo K., Ueno H., Costa A., Tanoi K., Matsumura H., Fujii-Kashino M., Horiuchi T., Nayef M.A., Shabala S., An G., Ma J.F., Horie T. (2017) OsHKT1;5 mediates Na^+ exclusion in the vasculature to protect leaf blades and reproductive tissues from salt toxicity in rice. Plant J **91**, 657-670.

27. Latha R. (2000) Studies on propagation, genetic relationship and characterization of salinity tolerance in *Porteresia coarctata* (Roxb.) Tateoka, a wild relative of rice. *Madras, India*, **132**, l.
28. Lebaudy A., Pascaud F., Véry A.-A., Alcon C., Dreyer I., Thibaud J.-B. & Lacombe B. (2010) Preferential KAT1-KAT2 heteromerization determines inward K^+ current properties in *Arabidopsis* guard cells. *Journal of Biological Chemistry*, **285**, 6265-6274.
29. Lomize M.A., Pogozheva I.D., Joo H., Mosberg H.I. & Lomize A.L. (2012) OPM database and PPM web server: resources for positioning of proteins in membranes. *Nucleic Acids Research*, **40**, D370-D376.
30. Martínez-Atienza J., Jiang X., Garciadeblas B., Mendoza I., Zhu J.-K., Pardo J.M. & Quintero F.J. (2007) Conservation of the salt overly sensitive pathway in rice. *Plant Physiology*, **143**, 1001-1012.
31. Mäser P., Hosoo Y., Goshima S., Horie T., Eckelman B., Yamada K., …, Oiki S. (2002) Glycine residues in potassium channel-like selectivity filters determine potassium selectivity in four-loop-per-subunit HKT transporters from plants. *Proceedings of the National Academy of Sciences*, **99**, 6428-6433.

32. Menguer P.K., Sperotto R.A. & Ricachenevsky F.K. (2017) A walk on the wild side: *Oryza* species as source for rice abiotic stress tolerance. *Genetics and Molecular Biology*, **40**,238-252.
33. Mian A., Oomen R.J., Isayenkov S., Sentenac H., Maathuis F.J. & Véry A.A. (2011) Over-expression of an Na^+-and K^+-permeable HKT transporter in barley improves salt tolerance. *The Plant Journal*, **68**, 468-479.
34. Mickelbart M.V., Hasegawa P.M. & Bailey-Serres J. (2015) Genetic mechanisms of abiotic stress tolerance that translate to crop yield stability. *Nature Reviews Genetics*, **16**, 237-251.
35. Munns R. & Tester M. (2008) Mechanisms of salinity tolerance. *Annual Review of Plant Biology,* **59,** 651-681.
36. Munns R., James R.A., Xu B., Athman A., Conn S.J., Jordans C., …, Tester M. (2012) Wheat grain yield on saline soils is improved by an ancestral Na^+ transporter gene. *Nature Biotechnology*, **30**, 360-364.
37. Negrão S., Almadanim C.M., Pires I.S., Abreu I.A., Maroco J., Courtois B., …, Oliveira M.M. (2013) New allelic variants found in key rice salt-tolerance genes: An association study. *Plant Biotechnology Journal*, **11**, 87-100.
38. Oh S.-J., Kim Y.S., Kwon C.-W., Park H.K., Jeong J.S. & Kim J.-K. (2009) Overexpression of the transcription factor AP37 in rice improves grain yield under drought conditions. *Plant Physiology*, **150**, 1368-1379.
39. Oostenbrink C., Villa A., Mark A.E. & Van Gunsteren W.F. (2004) A biomolecular force field based on the free enthalpy of hydration and solvation: the GROMOS force-field parameter sets 53A5 and 53A6. *Journal of Computational Chemistry*, **25**, 1656-1676.
40. Platten J.D., Cotsaftis O., Berthomieu P., Bohnert H., Davenport R.J. Fairbairn D.J., …, Tester M (2006) Nomenclature for HKT transporters, key determinants of plant salinity tolerance. *Trends in Plant Science*, **11**, 372–374.
41. Platten J.D., Egdane J.A. & Ismail A.M. (2013) Salinity tolerance, Na^+ exclusion and allele mining of *HKT1;5* in *Oryza sativa* and *O. glaberrima*: many sources, many genes, one mechanism? *BMC Plant Biology*, **13**, 32.
42. Ren Z.-H., Gao J.-P., Li L.-G., Cai X.-L., Huang W., Chao D.-Y., …,Lin H.-X. (2005) A rice quantitative trait locus for salt tolerance encodes a sodium transporter. *Nature Genetics*, **37**, 1141-1146.

43. Sengupta S. & Majumder A.L. (2010) *Porteresia coarctata* (Roxb.) Tateoka, a wild rice: a potential model for studying salt-stress biology in rice. *Plant, Cell & Environment*, **33**, 526-542.
44. Schneider T., & Stoll E. (1978). Molecular-dynamics study of a three-dimensional one-component model for distortive phase transitions. *Physical Review B*, **17**, 1302.
45. Shabala S. (2013) Learning from halophytes: physiological basis and strategies to improve abiotic stress tolerance in crops. *Annals of Botany,* **112,** 1209-21.
46. Shabala S., Bose J., & Hedrich R. (2014). Salt bladders: do they matter?. *Trends in Plant Science*, *19*(11), 687-691.
47. Su Y, Luo W, Lin W, Ma L, Kabir MH. (2015) Model of cation transportation mediated by high-affinity potassium transporters (HKTs) in higher plants. *Biological Pocedures Online*. **17**, 1.
48. Sunarpi Horie T., Motoda J., Kubo M., Yang H., Yoda K., …, Uozumi N (2005) Enhanced salt tolerance mediated by AtHKT1 transporter induced Na^+ unloading from xylem vessels to xylem parenchyma cells. *The Plant Journal* **44**, 928–938.
49. Thomson M.J., de Ocampo M., Egdane J., Rahman M.A., Sajise A.G., Adorada D.L., …, Singh R.K. (2010) Characterizing the Saltol quantitative trait locus for salinity tolerance in rice. *Rice* **3**, 148-160.
50. Tounsi S., Ben Amar S., Masmoudi K., Sentenac H., Brini F. & Véry A.-A. (2016) Characterisation of two HKT1;4 transporters from *Triticum monococcum* to elucidate the determinants of the wheat salt tolerance *Nax1* QTL. *Plant Cell Physiology* **57**, 2047–2057.
51. Uozumi N., Kim E.J., Rubio F., Yamaguchi T., Muto S., Tsuboi A., …, Schroeder J.I. (2000) The *Arabidopsis* HKT1 gene homolog mediates inward Na^+ currents in *Xenopus laevis* oocytes and Na^+ uptake in *Saccharomyces cerevisiae*. *Plant Physiology*, **122**, 1249-1260.

52. Véry A.A., Gaymard F., Bosseux C., Sentenac H. & Thibaud J.B. (1995) Expression of a cloned plant K+ channel in *Xenopus* oocytes: analysis of macroscopic currents. *The Plant Journal*, **7**, 321-332.

53. Vieira-Pires R.S., Szollosi A. & Morais-Cabral J.H. (2013) The structure of the KtrAB potassium transporter. *Nature*, **496**, 323-328.

54. Wolf M.G., Hoefling M., Aponte-Santamaría C., Grubmüller H. & Groenhof G. (2010) g_membed: Efficient insertion of a membrane protein into an equilibrated lipid bilayer with minimal perturbation. *Journal of Computational Chemistry*, **31**, 2169-2174.

55. Xu, B., Waters, S., Byrt, C. S., Plett, D., Tyerman, S. D., Tester, M., ... & Gilliham, M. (2018). Structural variations in wheat HKT1;5 underpin differences in Na^+ transport capacity. *Cellular and Molecular Life Sciences*, **75**, 1133-1144.

56. Yang C, Zhao L, Zhang H, Yang Z, Wang H, Wen S, Zhang, C., Rustgi, S., von Wettstein, D. and Liu B. (2014). Evolution of physiological responses to salt stress in hexaploid wheat. *Proceedings of the National Academy of Sciences*, **111**, 11882-11887.

57. Zarei, M., Shabala S., Zeng, F., Chen, X., Zhang S., Azizi M., …, Shabala L. (2019) Comparing kinetics of xylem ion loading and its regulation in alophytes ahnd glycophytes. *Plant and Cell Physiology*, doi: 10.1093/pcp/pcz205.

Legends

Figure 1. Phylogenetic relationship and tissue-specific expression of *OcHKT1*;5 (*Oryza coarctata*). (A) Phylogenetic relationship of OcHKT1;5 transporter with homologs from wheat and rice. The unrooted phylogenetic tree was constructed using full polypeptide sequences aligned with MUSCLE v3.8.31 (Edgar, 2004), and the Neighbor–Joining method with 1,000 bootstrap replicates, using PhyML version 20131022 software (http://phylogeny.lirmm.fr). The tree was drawn using Dendroscope (Huson *et al.,* 2007). Bootstrap values (percentages) are indicated at the corresponding nodes. The protein

(GenBank) accession numbers and species are listed in Supplementary Table S3. (B) Leaf and root specific *OcHKT1*;5 expression ($2^{-\Delta Ct}$) at 0h and 48h of salinity treatment. (C-D) qRT-PCR analysis of *OcHKT1*;5 expression in *O. coarctata* roots (C) and leaves (D) under salinity (150 mM NaCl). $2^{-\Delta Ct}$ and $2^{-\Delta\Delta Ct}$ values represent the mean ± standard deviation of six qRT-PCR assessments from two independent biological sample sets. Each qRT-PCR was carried out with three internal replicates. Significance was calculated using one way ANOVA (Graph Pad v. 6.0): * $P < 0.05$, ** $P < 0.01$, **** P<0.0001.

Figure 2. OcHKT1;5 shows Na^+-selective transport in yeast and *Xenopus* oocytes. (A-B) OcHKT1;5 expression in yeast. (A) Na^+ efflux-deficient yeast B31 strain expressing OcHKT1;5 was grown on AP-Gal medium (with adenine, tryptophan) and NaCl (0, 10, 25, 50 or 100 mM). Increasing NaCl concentration inhibits growth of B31 cells expressing OcHKT1;5 due to accumulation of Na^+ within cells. Yeast cells transformed with *pYES2* served as negative control. W303.1a: wild type yeast strain. Drop test shown is one of three biological replicates, each with two internal repetitions. (B) Growth of yeast cells expressing OcHKT1;5 in AP-Gal media (liquid) with increasing NaCl concentrations (0, 50, 100 mM), at 24 hours. Data is the mean (± SD) of three independent biological replicates, each with three internal replicates. Significance was calculated using one way ANOVA (Graph Pad v. 6.0): *** $P < 0.001$, **** P<0.0001. (C-E) Na^+ *versus* K^+ selectivity of OcHKT1;5 and OsHKT1;5-Ni expressed in *Xenopus* oocytes, analyzed by voltage-clamp. The current-voltage relationships were determined in bath solutions containing varying mixed concentrations of Na^+ and K^+ (Glu salts) at 0.3 or 10 mM. Oocytes were injected with water (C), OcHKT1*;5* cRNA (D), orOsHKT1;5-Ni cRNA (E). Current data are means ± SE. Number of biological replicates is three in (C) and (D) and four in (E).

Figure 3. OcHKT1;5 differs from OsHKT1;5-Ni by a lower affinity for Na^+ and higher maximal conductance. Effect of external Na^+ concentration (0.03, 0.3, 3, 10, 30 and 100 mM) on OcHKT1;5 (A) andOsHKT1;5-Ni (B) currents recorded in parallel in a same batch of transporter-expressing oocytes. (C) Reversal potential of currents through OcHKT1;5 andOsHKT1;5-Ni. Reversal potential of currents were determined graphically from current-voltage (I-V) relationships using the batch of oocytes from (A) and (B). Lines correspond to logarithmic fits of the reversal potential *versus* Na^+ activity relationships. (D) Effect of external Na^+ concentration on the macroscopic inward conductance of OcHKT1;5 and OsHKT1;5-Ni. Macroscopic inward conductances were determined (using the same batch of oocytes as above) as the slopes of the I–V relationships between the three I-V points closest to reversal potentials. Hyperbolic equations were fitted to inward conductance evolution with

external Na^+ (solid and dashed lines) to determine the apparent K_M (half-saturation concentration) and maximal inward conductance (Gmax). Fitted parameters were as follows: K_M = 32 mM and Gmax = 490 µS for OcHKT1;5; K_M= 2 mM and Gmax = 130 µS for OsHKT1;5-Ni. Data in (A) to (D) are means ± SE (n = 5 to 7), and are representative of two experiments performed in different oocyte batches.

Figure 4: Comparative electrostatic maps of the pore entrance of OcHKT1;5 and OsHKT1;5-Ni. (A, B) Model monomer top view of OsHKT1;5-Ni (A) and OcHKT1;5 (B) with coulombic calculations. Red denotes negative charge while blue denotes positive charge. Key residues or changes are highlighted. Pore entrance is seen, predominantly negative charged. Snapshots from the 20 mM NaCl monomer simulations show the arrangement of residues in the outer para loops just outside the entrance of the transporter pore for OsHKT1;5-Ni (C) and OcHKT1;5 (D). This arrangement is shown in the scheme below the snapshots (E, F; shaded grey region represents the ion translocation pore). The A subunit of HKT dimeric structure was used in OsHKT1;5 simulations, while the B subunit was used for OcHKT1;5 simulations, which is shown by the axis being rotated 180° in the OcHKT1;5 image.

Figure 5: Distance plots between charged sidechain atoms on the loops around the transporter pore entrance in OcHKT1;5 and OsHKT1;5-Ni at 10 mM NaCl (A, C) and 20 mM NaCl (B, D).

Figure 6: Effect of E270K and K239E reciprocal mutations on HKT1;5 currents in rice and *O. coarctata* respectively. Currents were recorded in *Xenopus* oocytes expressing (A) OsHKT1;5-Ni or the mutant transporter (OsHKT1;5-Ni E270K ; B) and (C) OcHKT1;5 or the mutant transporter (OcHKT1;5 K239E ; D), at different Na^+ concentrations (0.3, 3, 10, 30 and 100 mM). Currents were recorded in parallel in wild type and mutant transporters in the same batch of transporter-expressing oocytes. Data are means ± SE (n = 5 or 6;), and are representative of two experiments performed in different oocyte batches (separate from those in Fig. 3). (E, F) Macroscopic inward conductances were determined at the different Na^+ concentrations from currents recorded in oocytes expressing OsHKT1;5-Ni or the mutant transporter OsHKT1;5-Ni-E270K (E), and OcHKT1;5 or the mutant transporter OcHKT1;5-K239E (F). Data in (E) and (F) are means ± SE, and come from two experiments performed in different oocyte batches (n = 14 and 7 for wild type rice HKT1;5 (OsHKT1;5-Ni) and mutant (OsHKT1;5-Ni-E270K), respectively, n = 5 and 8 for wild type *O. coarctata* HKT1;5

(OcHKT1;5) and mutant OcHKT1;5-K239E respectively). Hyperbolic equations were fitted to inward conductance evolution with external Na^+ (solid lines) to determine the apparent K_M and maximal inward conductance (Gmax). Fitted parameters were as follows: for OsHKT1;5-Ni: K_M= 2 mM and Gmax = 145 µS; for OsHKT1;5-Ni-E270K: K_M= 6 mM and Gmax = 220 µS; for OcHKT1;5: K_M = 32 mM and Gmax = 490 µS; for OcHKT1;5-K239E: K_M = 3.5 mM and Gmax = 255 µS.

Figure 7: Xylem sap Na^+ (A) and K^+ (B) concentrations in *O. sativa* and *O. coarctata* plants exposed to 80 mM NaCl for a week. Mean ± SE (n= 3-6). In each panel, data labelled with different lower-case letters are significantly different at $P < 0.05$ or $P < 0.001$.

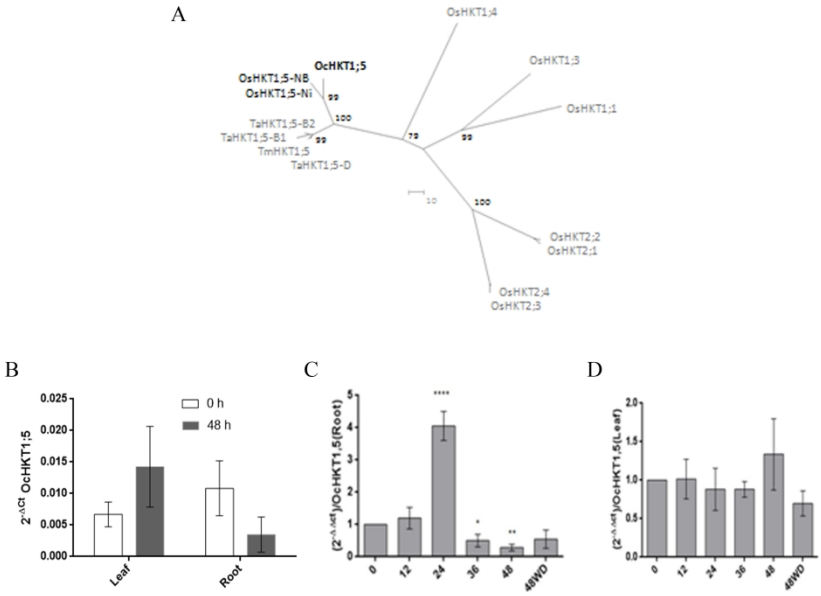

Figure 1

Fig 1

289x209mm (300 x 300 DPI)

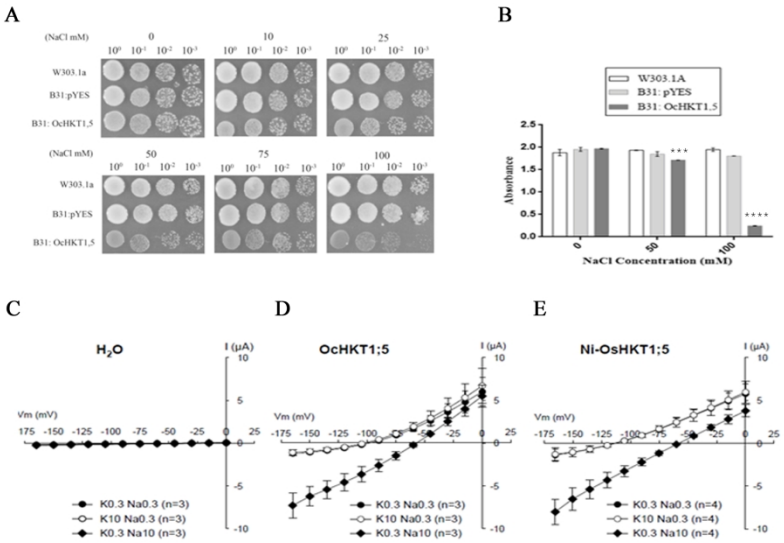

Figure 2

Fig 2

297x209mm (300 x 300 DPI)

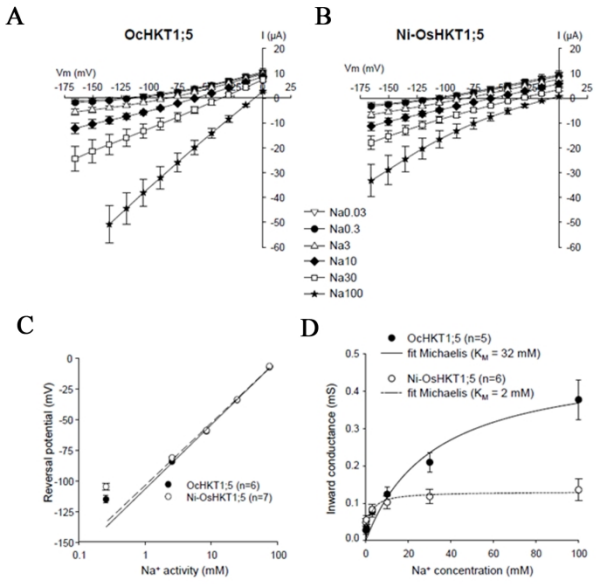

Figure 3

Fig 3

209x297mm (300 x 300 DPI)

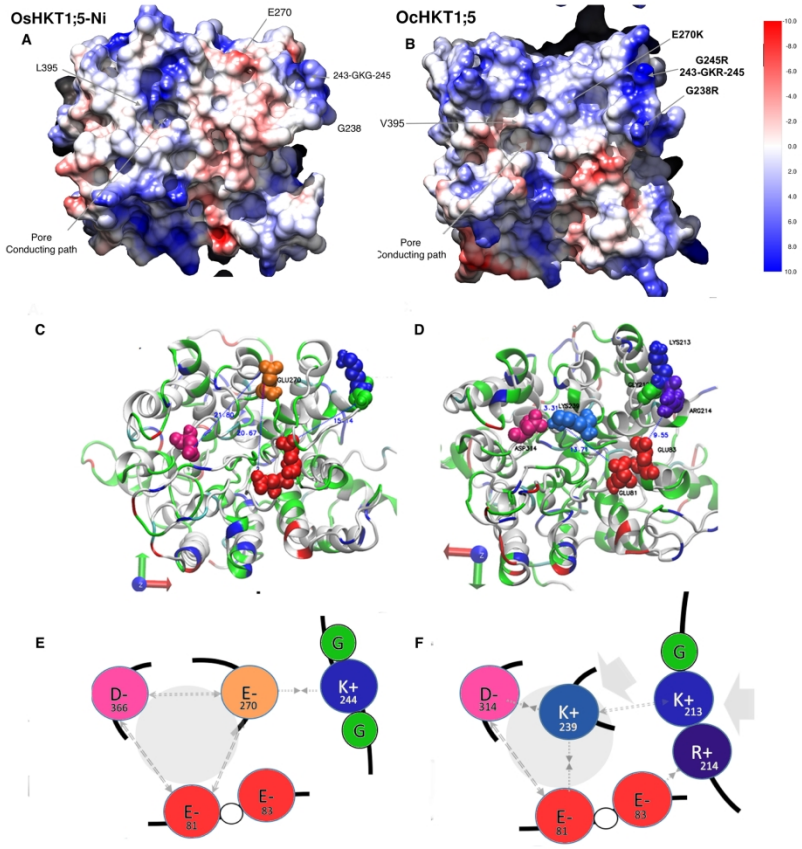

Fig 4

209x297mm (300 x 300 DPI)

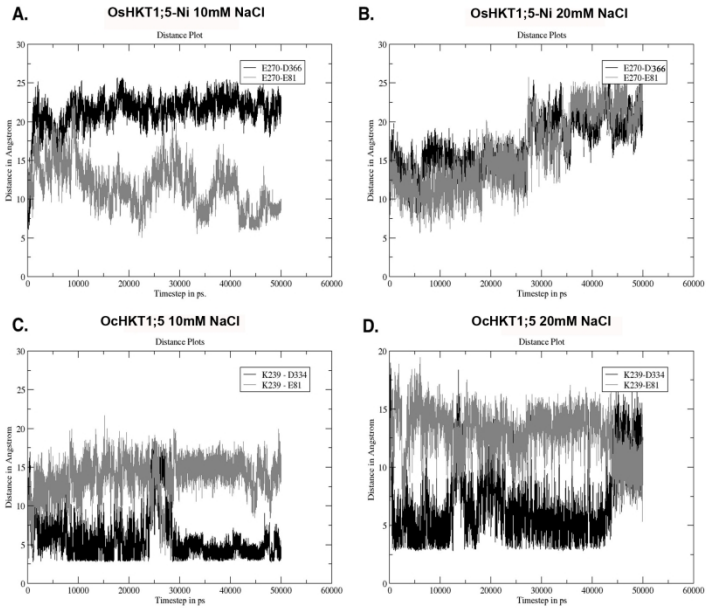

Figure 5

Fig 5

209x297mm (300 x 300 DPI)

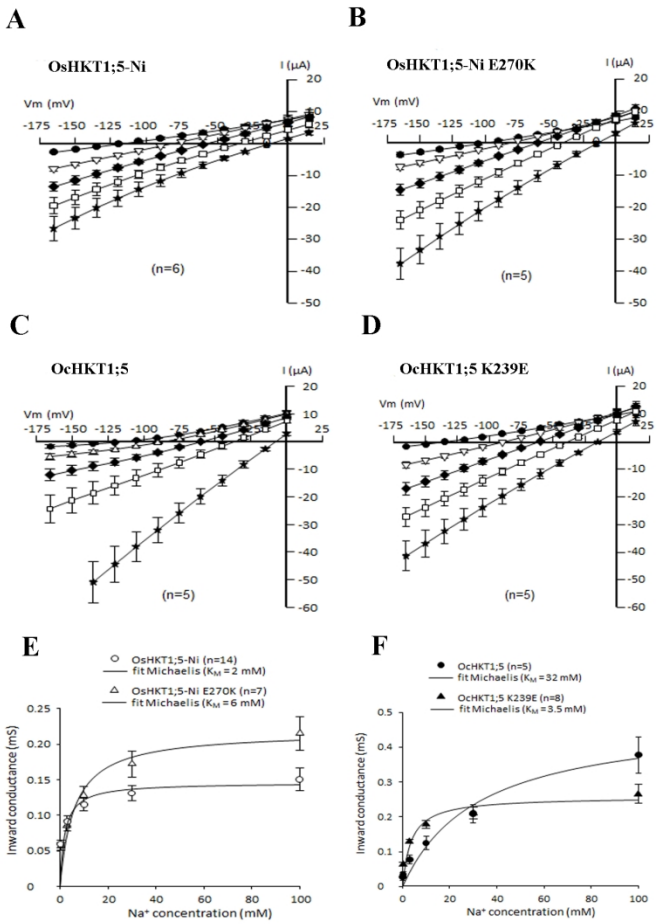

Figure 6

Fig. 6

147x209mm (300 x 300 DPI)

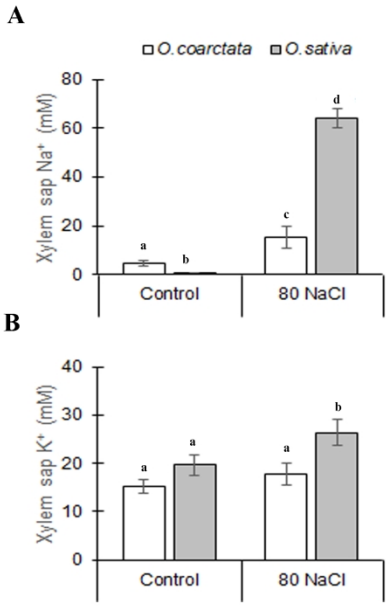

Figure 7

Fig. 7

209x297mm (300 x 300 DPI)